catalysts

MDPI

Article

The Effect of Y Zeolites with Different Pores on Tetralin Hydrocracking for the Production of High-Value Benzene, Toluene, Ethylbenzene and Xylene Products

Ce Xian [1,2], Yichao Mao [2,*], Xiangyun Long [2], Ziming Wu [1], Xiang Li [3] and Zhengkai Cao [1,*]

[1] Dalian Research Institute of Petroleum and Petrochemicals, SINOPEC, Dalian 116045, China; xiance.fshy@sinopec.com (C.X.); wuziming.fshy@sinopec.com (Z.W.)
[2] Research Institute of Petroleum Processing, SINOPEC, Beijing 100083, China; longxy.ripp@sinopec.com
[3] College of Chemical Engineering and Materials Science, Tianjin University of Science and Technology, Tianjin 300457, China; lixiang@tust.edu.cn
* Correspondence: maoyc.ripp@sinopec.com (Y.M.); xiaocao19910926@163.com (Z.C.)

Abstract: A series of Y zeolites with different pore properties was prepared as a support for hydrocracking catalysts for the production of BTEX (benzene, toluene, ethyl-benzene, and xylene) from tetralin. Some important characterizations, including N_2 adsorption–desorption, NH_3-TPD, Py-IR, and HRTEM, were applied to obtain the properties of different catalysts. Meanwhile, the tetralin hydrocracking performances of those catalysts were investigated on a high-pressure fixed-bed microreactor. The results showed that Si/Al ratio is the core property of zeolites and that the increase in the V_{micro}/V_{meso} of zeolites could facilitate the formation of BTEX products by hydrocracking tetralin. The method of hydrocracking tetralin was proposed. It was also found that the hydrogenation–cracking path was controlled by aromatic saturation thermodynamics, and strong acidity aided the backward shift of equilibrium temperature.

Keywords: Y zeolite; porosity; tetralin; hydrocracking; BTEX

Citation: Xian, C.; Mao, Y.; Long, X.; Wu, Z.; Li, X.; Cao, Z. The Effect of Y Zeolites with Different Pores on Tetralin Hydrocracking for the Production of High-Value Benzene, Toluene, Ethylbenzene and Xylene Products. *Catalysts* **2022**, *12*, 848. https://doi.org/10.3390/catal12080848

Academic Editors: Maja Milojević-Rakić and Danica Bajuk-Bogdanović

Received: 1 July 2022
Accepted: 30 July 2022
Published: 2 August 2022

1. Introduction

With the continuous implementation of the carbon-neutrality policy and the development trend in energy transformation, the petrochemical industry has undergone great changes in terms of product structure adjustment and the nature of the products produced. From a long-term perspective, the demand for transport fuel will gradually decrease. In addition, the severity of the use of crude oil continues to worsen, which is a greater challenge for the petroleum processing and refining industry.

Light cycle oil (LCO), with a boiling point similar to that of diesel, is derived from fluid catalytic cracking, which has high aromatic, sulfur, and nitrogen contents, as well as a low cetane index [1,2]. There is a large gap between the nature of LCO and the China national VI diesel standard. If LCO is used to produce the blending component of clean diesel fuel, it will consume a large amount of hydrogen and cause high CO_2 emissions, which means it does not meet the requirements of environmental protection policies, the process is not economical, and the product has low commercial value. Therefore, many researchers use LCO, which is rich in aromatic hydrocarbons, to produce high-octane gasoline and light aromatic BTEX (benzene, toluene, ethyl-benzene, and xylene) components through selective hydrocracking technology [3,4]. This process can effectively reduce hydrogen consumption and greatly improve the commercial value of the product. To date, many institutions have developed a number of technologies using this principle, such as FD2G, RLG, and LCO-X.

According to previously reported research, most of the poly-aromatics in LCO are di-aromatic hydrocarbons. Researchers have investigated the reaction regularity of model

compounds, such as naphthalene and tetralin, and have studied the reactivity of hydro cracking catalysts [5,6]. Sato et al. [7] explored the hydrocracking of tetralin over NiW/USY catalysts; the reaction mechanisms of tetralin were investigated according to the product distribution, and they highlighted the importance of strengthening the connection between the active hydrogenation site and the acid site to improve the performance of the catalyst. Active metal components are the source of hydrogenation activity. Typically, noble metals and non-noble metal mixtures are used to hydrocrack catalysts. Noble metals can provide much higher hydrogenation activity; however, they are sensitive to S and N compounds and are easily poisoned to the point of deactivation. They are not suitable for LCO feeds with high sulfur content. Upare et al. [8] compared a monometallic Mo/Beta catalyst and bimetallic CoMo/Beta catalyst in the selective hydrocracking of tetralin into monocyclic aromatic hydrocarbons; the results indicated that the bimetallic CoMo Beta catalyst not only improved the catalytic activity in hydrocracking reactions but also showed better long-term stability. This study revealed that CoMo/Beta with SiO_2/Al_2O_3 of 25 gave the highest desired mono-aromatic hydrocarbon yield of 62.6% at the 99.5% conversion of tetralin for more than 140 h of reaction time. Laredo et al. [9] used tetralin to explore the effect of an $NiMo/Al_2O_3$/ZSM-5 catalytic system and operating conditions on BTX formation. It was disclosed that high BTX selectivity in the liquid phase with suitable tetralin conversion could be achieved using this catalytic system. One reason for this result is that Ni-Mo can effectively reduce coke formation and minimize catalysts' deactivation. Cao et al. [10] studied the selective hydrocracking of naphthalene and tetralin into mono-aromatic hydrocarbons over NiMo-AY and CoMo-AY grading catalysts. The results showed that the CoMo catalyst could hydro-saturate more naphthalene to tetralin but exhibit a lower yield of light aromatics. The NiMo catalyst presented higher selectivity in converting naphthalene into cyclanes. A CoMo-AY/NiMo-AY catalyst grading system with low carbon deposition and high stability was shown to be capable of maintaining a high percentage of active phases, which was more efficient in the conversion of LCO to high-octane gasoline.

The carrier of hydrocracking catalysts is not only the source of acid sites, but also, reactant and product diffusion depend on it. As has been previously reported, commonly used carrier types mainly include Y zeolite [11], Beta zeolite, ZSM-5 zeolite [12], MCM-41 zeolite, γ-Al_2O_3, and amorphous silica alumina (SiO_2-Al_2O_3) [13]. Some researchers have studied the conversion of LCO over porous aromatic framework carrier catalysts [14]. Each catalyst carrier has different acid properties and pore characteristics, thus showing different reaction characteristics [15]. Researchers have used a variety of modification methods to optimize the performance of carriers [16,17]. Nakajima et al. [18] used a variety of zeolites to study the activity and selectivity of the tetralin ring-opening reactions; the influence of the acidity and textural properties of the zeolites on the activity and selectivity was shown. The results showed that a 12-ring on the BEA zeolite and strong Brønsted acid sites exhibited higher tetralin conversion; moreover, BEA zeolites increased the number of Brønsted acid sites while maintaining the selectivity. Ren et al. [19] used fluorination−alkaline treatment-modified USY zeolites as the carrier of the hydrocracking catalyst and studied the hydrogenation and ring-opening performance of naphthalene. The results showed that the modified USY zeolite increased the volume of mesopore and pore diameter and increased the number of strong acid sites. The ring-opening product yield of the naphthalene hydrocracking reaction was greatly increased, and the content of poly-aromatics was effectively reduced. Youngseok et al. [20] used a combination of H-ZSM-5, H-Beta, and mesoporous H-Y zeolite as a carrier for the hydrocracking catalysts. Their study revealed that the tetralin conversion rate was 97.4%, and the total yields of BTX and alkylbenzenes were close to 56.1%. This was due to the fact that hybrid zeolite contains a 10-ring channel, 12-ring channel, and mesopores, while the appropriate acid properties aid the production of a much higher yield of BTX-rich light aromatics. Above all, there are many ways to adjust the channel structure of a catalyst carrier. However, the topological structure and specific characteristics of different carriers vary greatly, and the influence

of other properties, especially acid properties, cannot be explained when exploring the influence of catalyst pore properties.

As reported, Y zeolite, which is the main carrier of industrial hydrocracking catalysts, has a suitable pore structure, adjustable acidity, and favorable stability. In order to reduce the influence of the acidic properties of a carrier, Y zeolite was modified using appropriate methods, and two series of Y zeolites with similar acid properties but significantly different pore structures were prepared, and the hydrocracking catalyst was prepared using these Y zeolites as carriers. The influence of the pore properties of Y zeolite on the selective hydrocracking of tetralin to produce light aromatics was investigated. The influence of Y zeolite's pore characteristics on the key conversion steps of tetralin was clarified, which played a guiding role in the development of hydrocracking catalysts.

2. Results and Discussion

2.1. Characterization of Zeolites and Catalysts

Y zeolite has a different order of Si–O–Al or Si–O–Si linkages in the framework, and the molar Si/Al ratio of zeolite result in variations in the acidity of the Si(OH)Al group [21]. The acid properties of Y zeolites are mainly related to the content and distribution of aluminum atoms. Moreover, the amount of aluminum in the framework affects the unit cell constant. In this work, a series of zeolite Y was divided into two parts according to the value of the Si/Al ratio characterized by the XRF and the unit cell constant characterized by the XRD, as shown in Table 1 and Figure 1.

Table 1. Unit cell constant of zeolite Y1–Y8.

Sample	Si/Al	Unit Cell Constant/(Å)	Sample	Si/Al	Unit Cell Constant/(Å)
Y1	7.88	24.39	Y5	3.34	24.56
Y2	8.89	24.32	Y6	3.68	24.62
Y3	8.40	24.37	Y7	3.59	24.54
Y4	8.25	24.35	Y8	3.49	24.65

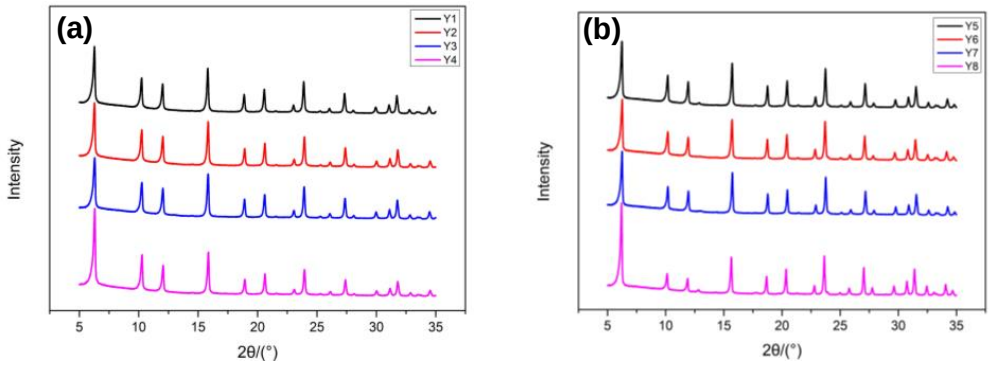

Figure 1. (**a**) XRD patterns of Y1–Y4 and (**b**) XRD patterns of Y5–Y8.

The key factor determining both the unit cell constant and acidity is the Si/Al ratio of zeolites. It can be seen from Table 1 that the Si/Al ratio and the unit cell constants of Y1–Y4 zeolites were very similar, and the Si/Al ratio and the unit cell constants of Y5–Y8 zeolites were also relatively similar. This means that the acidities of the samples may have been similar in each group. From Figure 1, it can be seen that each group of samples showed a typical Y zeolite crystal structure, indicating that the framework structure of all the samples was not destroyed. NH_3-TPD was used to estimate the acid site strength distribution using a single temperature programmed desorption method; desorption peaks at less than 200 °C, 200–350 °C and higher than 350 °C represented the acidic sites with weak strength, medium strength, and high strength [22]. The results are shown in Figure 2.

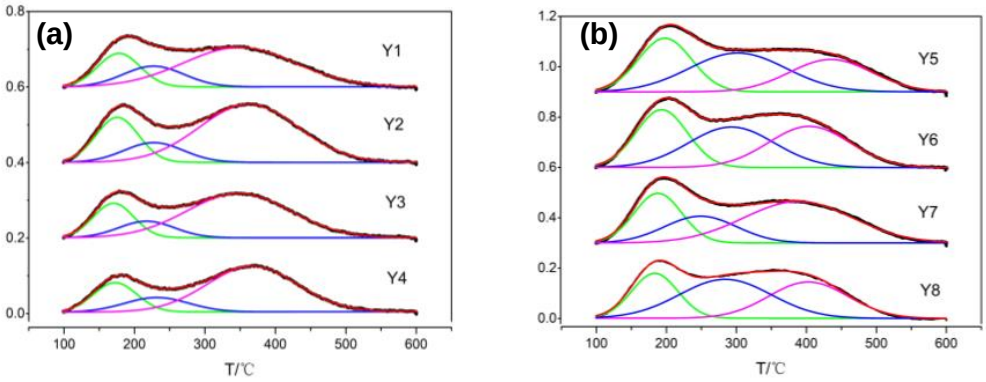

Figure 2. (**a**) NH_3-TPD profiles of Y1–Y4 and (**b**) NH_3-TPD profiles of Y5–Y8. Black line: the desorption peak of zeolite acid sites obtained by testing. Green line: the desorption peak of weak acid sites obtained by fitting. Blue line: the desorption peak of medium acid sites obtained by fitting. Pink line: the desorption peak of strong acid sites obtained by fitting. Red line: the desorption peak of zeolite acid sites obtained by fitting.

In order to further analyze the difference in the acid strength of each sample, the profiles in Figure 2 were treated according to the highest degree of fitting, and the acid amount was calculated according to the peak area and the desorption ammonia titer. The results are shown in Table 2.

Table 2. Acid strength distribution of Y1–Y8.

Sample	Total Acid Amount /(μmol·g^{-1})	Weak Strength /(μmol·g^{-1})	Medium Strength /(μmol·g^{-1})	Strong Strength /(μmol·g^{-1})
Y1	1400	280	230	890
Y2	1620	330	230	1060
Y3	1470	300	190	980
Y4	1500	300	220	980
Y5	1860	520	810	530
Y6	1950	500	780	670
Y7	1840	470	650	720
Y8	1920	450	870	600

It can be seen from Table 2 that the total acid amounts of the samples could also be divided into two groups according to the unit cell constant, and the acidities of zeolites within each group were very similar. The total acid amounts in theY5, Y6, Y7 and Y8 samples were higher than those in the Y1, Y2, Y3, and Y4 samples. However, the amounts of strong acid in Y5, Y6, Y7, and Y8 were lower than those in the Y1, Y2, Y3, and Y4 samples; a similar trend was shown in the Si/Al ratios. Therefore, it can be concluded that a high ratio of Si and Al can facilitate more strong acid sites but fewer total acid sites.

The standard deviation of most samples was less than 10%. In terms of the different strengths of acidity, Y1, Y2, Y3, and Y4 were classified as strong acid zeolites (SAZ), and Y5, Y6, Y7, and Y8 could be defined as medium acid zeolites (MAZ). In a comparison between SAZ and MAZ, it was indicated that the medium acid sites may be converted from strong ones in the preparation of zeolite dealumination to reduce the unit cell constant. The IR spectra of pyridine adsorbed onto zeolite at various temperatures is usually used to identify the Brϕnsted acid sites and Lewis acid sites with different strengths [23]; the results are shown in Table 3.

Table 3. Py-IR results of Y1–Y8.

Sample	200 °C		350 °C	
	L Acid Amount /(μmol·g^{-1})	B Acid Amount /(μmol·g^{-1})	L Acid Amount /(μmol·g^{-1})	B Acid Amount /(μmol·g^{-1})
Y1	155	282	118	239
Y2	81	533	65	482
Y3	75	428	64	385
Y4	34	323	34	320
Y5	39	480	24	412
Y6	30	641	19	531
Y7	13	550	9	486
Y8	22	589	12	537

Table 3 suggests that the zeolites could still be divided into two parts according to the Brϕnsted acid sites and Lewis acid sites; the difference in the acid amount in the SAZ series was small after Y1 was removed. The MAZ produced similar results when Y7 was removed. Compared with MAZ, the SAZ had more Lewis acid and less Brϕnsted acid, which was quite different to the NH_3-TPD results. The differences within each group were also higher than those observed in the NH_3-TPD results. This can be attributed to the different absorbed molecular sizes of ammonia and pyridine. Through external and internal diffusion, the probe molecule could reach distinct active sites for absorption; therefore, the difference was usually due to the porous property of zeolites. The isotherms of nitrogen physisorption and the pore size distribution of the Y zeolites are presented in Figures 3 and 4.

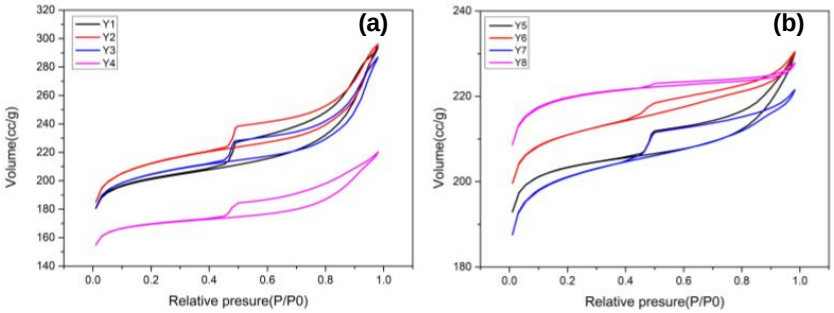

Figure 3. The isotherms of nitrogen physisorption of zeolites (**a**) Y1–Y4 and (**b**)Y5–Y8.

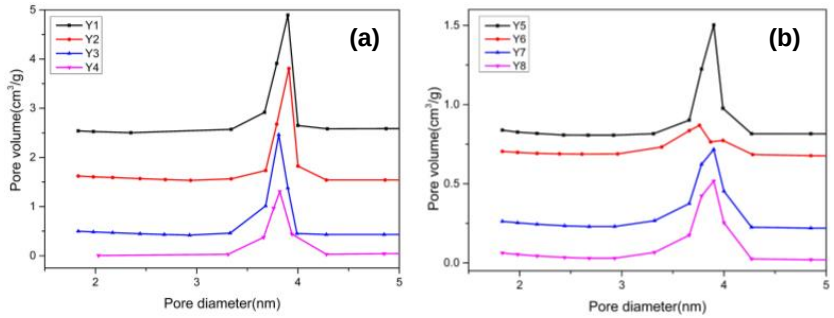

Figure 4. The pore size distribution of zeolites (**a**) Y1–Y4 and (**b**)Y5–Y8.

It can be clearly seen that the N_2 adsorption–desorption isotherms of all the zeolites were type IV with a typical H_2 type hysteresis loop, indicating that these zeolites possess microporous and mesoporous structures [24]. The porous properties are shown in Table 4.

Table 4. Porosity of Y zeolites.

Sample	S_{BET}/ ($m^2 \cdot g^{-1}$)	S_{micro}/ ($m^2 \cdot g^{-1}$)	S_{meso}/ ($m^2 \cdot g^{-1}$)	V_{total}/ ($mL \cdot g^{-1}$)	V_{micro}/ ($mL \cdot g^{-1}$)	V_{meso}/ ($mL \cdot g^{-1}$)	V_{micro}/ V_{meso}
Y1	571	537	34	0.34	0.25	0.09	2.77
Y2	681	609	72	0.45	0.28	0.17	1.64
Y3	694	640	54	0.44	0.30	0.14	2.14
Y4	721	659	62	0.46	0.31	0.15	2.06
Y5	708	678	30	0.37	0.32	0.05	6.40
Y6	678	650	28	0.34	0.30	0.04	7.50
Y7	682	662	20	0.36	0.31	0.05	6.20
Y8	704	690	14	0.34	0.31	0.03	10.33

The results from Table 4 show that, in SAZ, the S_{micro} increased while the S_{meso} changed randomly; in the MAZ series, the opposite was observed. In addition, the Y8 zeolite showed a significantly high value of V_{micro}/V_{meso}, which could also be verified from the super flat hysteresis loop in Figure 4b.

Due to the high surface tension in the capillary condensation process, transition metal compounds are usually located on the outer surfaces of catalyst microparticles during wet impregnation preparation of the catalyst and further form layered sulfides in the sulfidation process. The sizes of bulk particles from active metal sulfides are usually used to identify the hydrogenation activity of catalysts [25]; here, the catalysts in the sulfide form were investigated using the HRTEM method. Figure 5 shows microphotographs of the catalysts, and the average particle length ($\overline{L}$) and stacking number ($\overline{N}$) were calculated, as shown in Table 5.

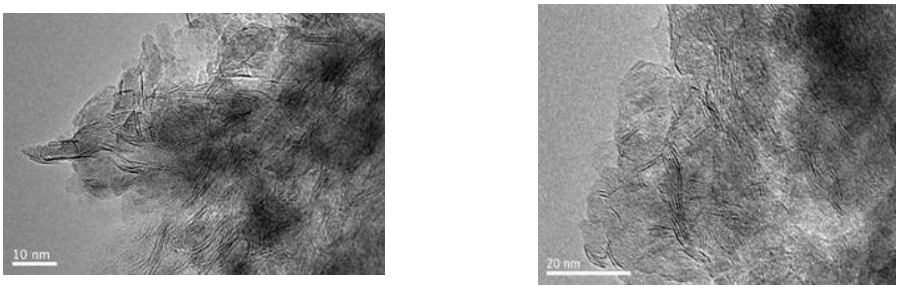

(**a**) (**b**)

Figure 5. HRTEM images of sulfide catalysts (**a**) CAT3 and (**b**) CAT7.

Table 5. The average particle length ($\overline{L}$) and stacking number ($\overline{N}$) of CAT3 and CAT7.

Simple	Average Particle Length ($\overline{L}$)/nm	Average Stacking Number ($\overline{N}$)
CAT3	5.91	1.99
CAT7	5.67	1.73

The particle length and stacking number values were close to the results found in common hydrocracking catalysts [26]. The size of bulk particles from the Y7 sample was slightly smaller than that of Y3; this can be explained by the fact that there were stronger Brϕnsted sites, which led to strong metal–support interaction, which ensured it was easy to retain the single-layer structure during the sulfidation and reaction procedure.

2.2. Hydrocracking of Tetralin

Tetralin hydrocracking over catalysts takes place through a complex reaction scheme, as shown in Figure 6, which is related to this research [7,27].

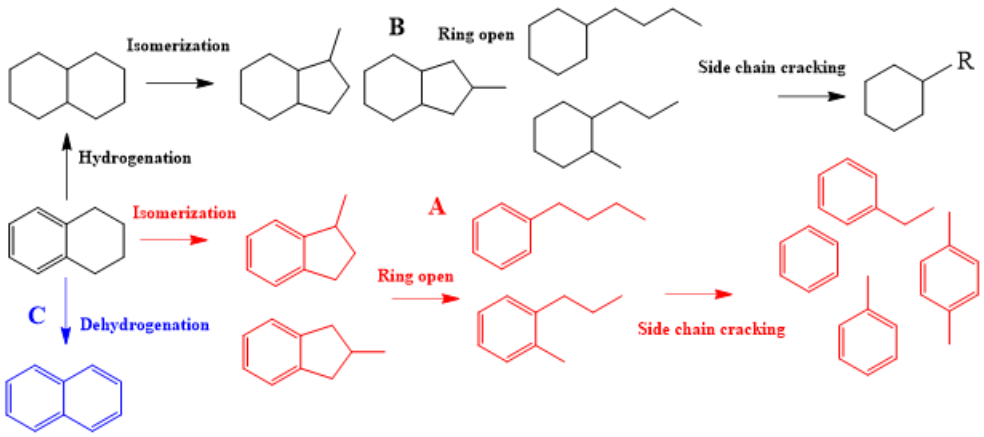

Figure 6. Reaction scheme for tetralin hydrocracking over bifunctional catalysts. A: Isomerization-cracking; B: hydrogenation-cracking; and C: dehydrogenation.

The hydrocracking of tetralin is based on the mechanism of a carbonium reaction, including hydrogenation, isomerization, β cracking, and dehydrogenation. In addition to hydrogenation, tetralin can undergo naphthenic ring isomerization or dehydrogenation; these schemes are differentiated in the first step in the reaction of tetralin. In path A and B, the naphthenic ring opens, followed by cracking reactions to form BTEX or single naphthenic compounds. To facilitate the analysis of the results of the catalytic tests, the identified compounds were assembled in different groups, as indicated in Table 6.

Table 6. Compounds assembled in different groups.

Group	Compounds
HEAVY	naphthalene, alkyl-naphthalene
ARO-ISO	methyl-indan
ARO-RO	butyl-benzene, methylpropenyl-benzene
ARO-C	benzene, toluene, xylenes, ethyl-benzene
H	decalin
HYD-RO	butyl-cyclohexane, methyl-butylcyclopentane
HYD-C	methyl-cyclopentane, ethyl-cyclohexane

In order to reasonably explain the influence of the pore properties of Y zeolite on the hydrocracking process of tetralin, the conversion rates, yields of products and selectivity are defined by the following:

$$C_{tetralin} = \frac{\omega_i - \omega_f}{\omega_i} \times 100\% \quad (1)$$

where ω_i and ω_f represent the content of tetralin in the material and the product, respectively.

$$Y_{iso-cracking} = \sum \omega_{ARO-ISO} + \omega_{ARO-RO} + \omega_{ARO-C} \quad (2)$$

$$Y_{hydro-cracking} = \sum \omega_H + \omega_{HYD-RO} + \omega_{HYD-C} \quad (3)$$

$$Y_{BTEX} = \sum \omega_{ARO-C} \quad (4)$$

$$Y_{heavy} = \sum \omega_{HEAVY} \quad (5)$$

$$S_{iso-cracking} = \frac{Y_{iso-cracking}}{C_{tetralin}} \times 100\% \quad (6)$$

$$S_{heavy} = \frac{\omega_{HEAVY}}{C_{tetralin}} \times 100\% \quad (7)$$

$$S_{ring-opening} = \frac{\omega_{ARO-RO} + \omega_{ARO-C}}{C_{tetralin}} \times 100\% \quad (8)$$

$$S_{sidechain-cracking} = \frac{\omega_{ARO-C}}{C_{tetralin}} \times 100\% \quad (9)$$

Tetralin hydrocracking conversion over different catalysts is shown in Figure 7a,b. It can be seen that the conversion of tetralin obviously increased with the increase in temperature, and the conversion of the SAZ group was significantly higher than that of the MAZ group at the same temperature. This was mainly due to the high Si/Al ratio in the SAZ group, which had higher strong acid strength. Sato et al. [7] also found that a higher ratio of strong acid sites contributes to the improvement in the conversion depth of tetralin. In the SAZ group, the conversion of tetralin was mainly proportional to S_{BET} and V_{total}. In the MAZ group, it can be seen that CAT5 displayed higher conversion than the others, and this was mainly due to the high S_{BET} and V_{total} of Y5. Moreover, it can be seen that the conversion curve converged in the high reaction temperature for CAT6, CAT7 and CAT8; this indicated that the reaction barrier was overcome by the diffusion improvement [28].

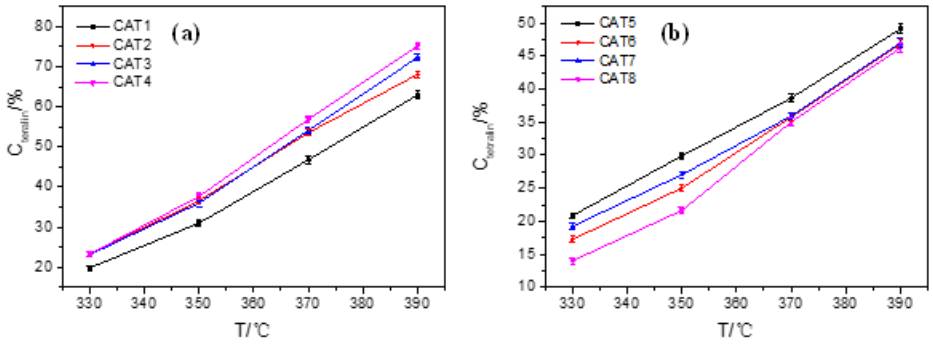

Figure 7. The relationship of conversion and temperature over catalysts (**a**) CAT1–CAT4 and (**b**) CAT5–CAT8.

Figure 8 shows the relationship between $Y_{iso-cracking}$ and temperature over different catalysts. When the reaction temperature was 330 °C and 350 °C, the $Y_{iso-cracking}$ values of the SAZ and MAZ group were similar. When the reaction temperature rose to 370 °C and 390 °C, the $Y_{iso-cracking}$ value of the SAZ group was higher than that of the MAZ group. It can be seen that a higher temperature and more strong acid sites can facilitate the occurrence of the iso-cracking reaction. Strong acid strength is more conducive to the occurrence of the iso-cracking reaction pathway, and the SAZ group with a higher Si/Al ratio performed better. From Figure 8a, it is obvious that the $Y_{iso-cracking}$ value of CAT4 was lower than that of the others, and the $Y_{iso-cracking}$ values of CAT1, CAT2, and CAT3 were similar. This may have been related to pore size distribution. It can be seen from Figure 4 that Y1, Y2, and Y3 had concentrated pore size distributions which were all concentrated from 3.5 nm to 4.0 nm. The pore size distribution of Y4 was relatively dispersed, which was not conducive to the diffusion reactants. From Figure 8a, it can be seen that the $Y_{iso-cracking}$ values of CAT6, CAT7, and CAT8 were more similar. In terms of the pore distribution, Y7 and Y8 had similar pore concentration characteristics; their $Y_{iso-cracking}$ value was consistent at 390 °C.

Figure 9 shows a comparison of the yields of BTEX in the SAZ group and MAZ group; it can be seen that the yields the two groups were similar. Generally, there are two main reasons for this. One reason is that in terms of acidity, ring-opening and sidechain-breaking reactions in the iso-cracking pathway do not require many strong acid sites, and more medium acid sites are favorable for the occurrence of these two ideal reactions. This is easily illustrated by the Si/Al ratio of the zeolites: the MAZ group had a lower Si/Al ratio and more moderate acid strength and B-acid content, which are very favorable characteristics for both reaction paths. The other reason is the effect of pore properties. From Table 4, it can be seen that the V_{total} and V_{meso} of the SAZ group were larger than

those of the MAZ group, and the V_{micro} of the MAZ group was larger than that of the SAZ group. Trends in the yields of BTEX in the SAZ group and MAZ group were similar to the yields of iso-cracking. However, the MAZ group could produce semblable yields of BTEX, which means that the presence of more micropores is beneficial to the ring-opening and sidechain-breaking reactions.

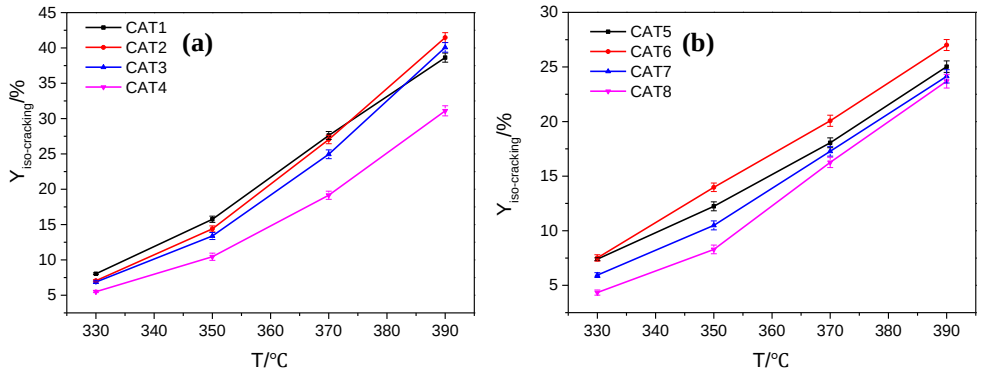

Figure 8. The relationship of yields of iso-cracking and temperature over catalysts (**a**) CAT1–CAT4 and (**b**) CAT5–CAT8.

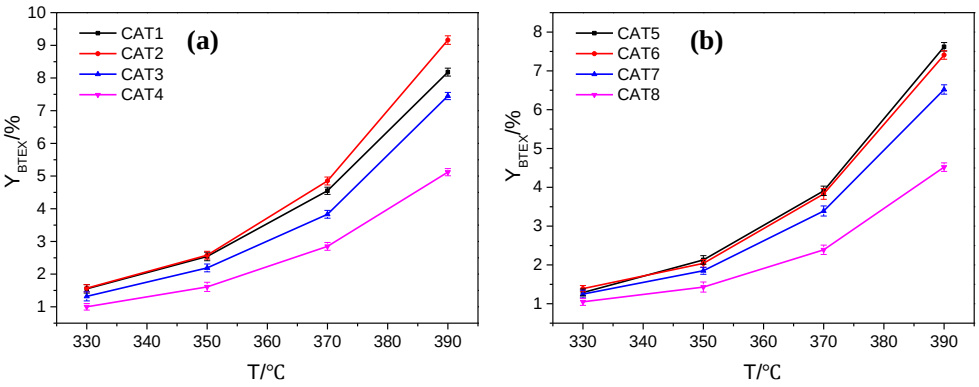

Figure 9. The relationship of yields of BTEX and temperature over catalysts (**a**) CAT1–CAT4 and (**b**) CAT5–CAT8.

The hydro-cracking reaction pathway is an important component of tetralin conversion. Figure 10 shows $Y_{hydro-cracking}$ over different catalysts. The $Y_{hydro-cracking}$ of all the catalysts increased first and then decreased. This inflection point is mainly related to the thermodynamics of aromatics saturation [29]. It can be seen that the SAZ group had the highest $Y_{hydro-cracking}$ value at 370 °C, and most catalysts in the MAZ group had the highest $Y_{hydro-cracking}$ value at 350 °C. This shows that the acid properties of zeolite directly affect the hydro-cracking pathway performance of tetralin. Strong acid sites in zeolites help to delay the aromatics saturation point; therefore, a suitable Si/Al ratio is necessary to reduce the selectivity of the hydro-cracking reaction pathway of aromatics, and this feature can be effectively used to design the development of related catalysts.

The dehydrogenation reaction is the main source of heavy aromatics. From Figure 11, it can be seen that Y_{HEAVY} is proportional to the reaction temperature. This is because the dehydrogenation reaction is endothermic, and raising the temperature favors dehydrogenation. Moreover, the Y_{HEAVY} of the SAZ group was larger than that of the MAZ group. This is mainly because the SAZ group had a higher Si/Al ratio and higher acid strength, which provided suitable conditions for the dehydrogenation reaction. Gutiérrez et al. [30] investigated the role of acid sites in LCO hydrogenation and coking deactivation; it was found that strong acid sites are considered to be the main coking sites of LCO, and there is a linear relationship between the amount of coking and the number of strong acid sites. In the SAZ group, their V_{meso} was larger than that of the MAZ group, and more mesoporous

pores provided a reaction space for dehydrogenation. Y2 and Y4 had lower V_{micro}/V_{meso} than Y1 and Y3; this was consistent with the higher yield of CAT2 and CAT4.

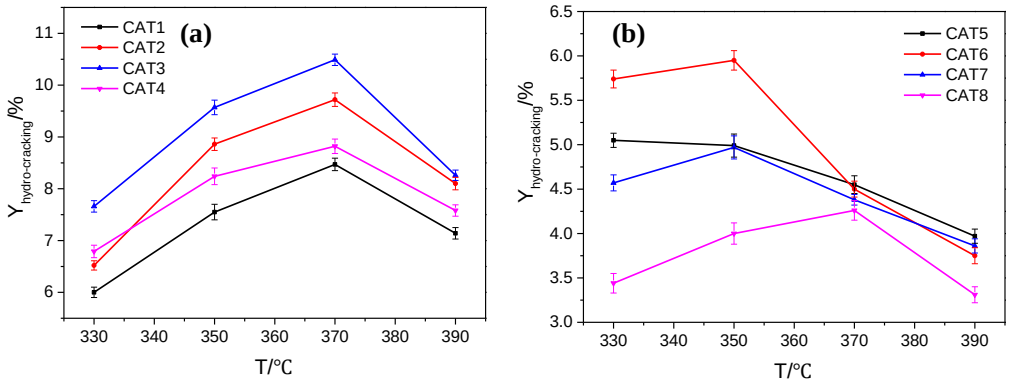

Figure 10. The relationship between yields of $Y_{hydro-cracking}$ and temperature over catalysts (**a**) CAT1–CAT4 and (**b**) CAT5–CAT8.

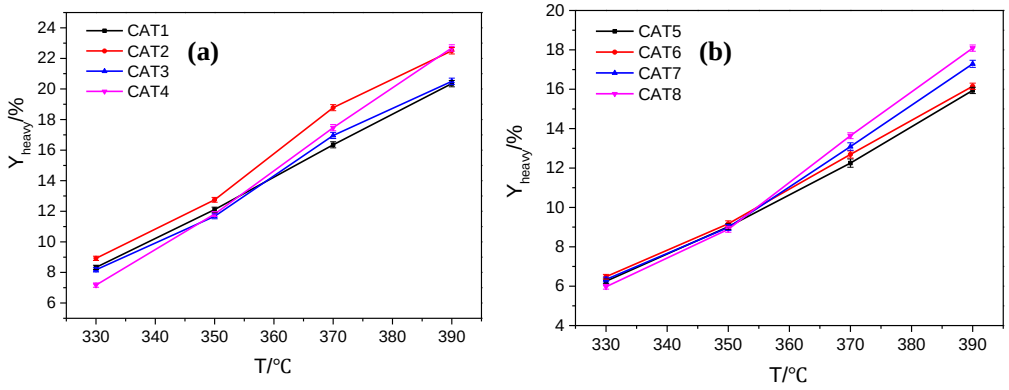

Figure 11. The relationship between yields of Y_{heavy} and temperature over catalysts (**a**) CAT1-CAT4 and (**b**) CAT5-CAT8.

By comparing the conversion rate of tetralin and the yield of product, it was found that the size of the micropores and mesopores was the main influencing factor in zeolites with similar acid properties. The presence of more micropores in zeolites is favorable to the formation of BTX products, and the presence of more mesopores is favorable to the dehydrogenation reaction. Therefore, the relationship between microporous and mesoporous molecular sieves should be adjusted to a reasonable range.

In order to investigate the effect of the microporous and mesoporous relationship on reaction selectivity, the selectivity at the same conversion rate was calculated. Due to the high activity of the SAZ series, the selectivity at a 60% conversion rate was calculated and correlated with the pore properties. The conversion of the MAZ series was low even at a high reaction temperature, so 45% conversion was used as the benchmark; the results are shown in Figures 12 and 13.

From the results shown in Figures 12 and 13, it can be seen that although acid properties display a certain influence, the selectivity of the catalyst and the ratio of V_{micro}/V_{meso} still correspond well. With the increase in V_{micro}/V_{meso}, the dehydrogenation selectivity increased and the isomerization cracking selectivity decreased. The isomerization selectivity of the MAZ molecular sieve reached a constant value faster. The selectivity of ring-opening and selectivity of sidechain-breaking decreased almost synchronously.

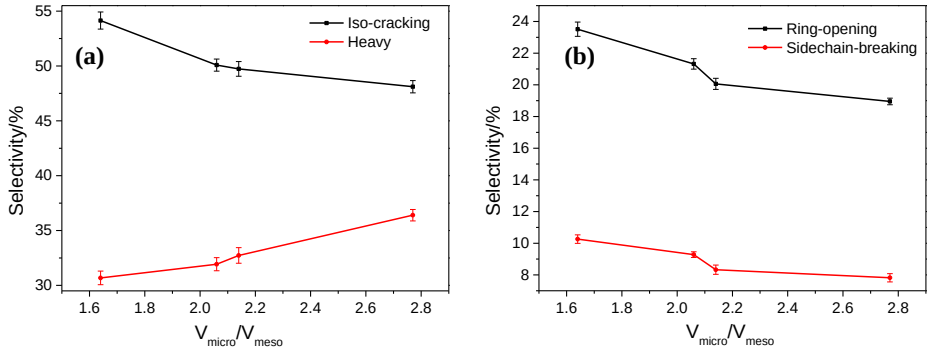

Figure 12. The path selectivity of SAZ zeolite at 60% conversion rate vs. V_{micro}/V_{meso}. (**a**) The selectivity of Iso-cracking and Heavy vs. V_{micro}/V_{meso} and (**b**) The selectivity of Ring-opening and Sidechain-breaking vs. V_{micro}/V_{meso}.

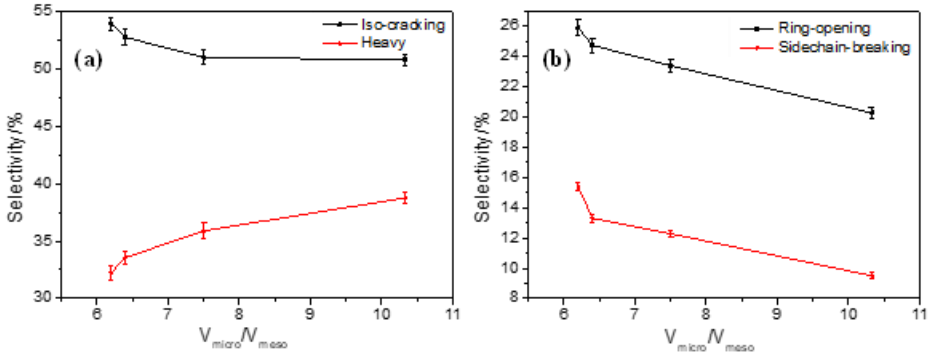

Figure 13. The path selectivity of MAZ zeolite at 45% conversion rate vs. V_{micro}/V_{meso}. (**a**) The selectivity of Iso-cracking and Heavy vs. V_{micro}/V_{meso} and (**b**) The selectivity of Ring-opening and Sidechain-breaking vs. V_{micro}/V_{meso}.

3. Materials and Methods

3.1. Materials

The following reagents were used without further purification: USY zeolite (Sinopec Catalyst Co., Ltd., Beijing, China), The eight USY zeolites that were labeled Y1, Y2, Y3, Y4, Y5, Y6, Y7, and Y8 were Pseudoboehmite (SB, SASOL), Tetralin (98%, ACROS), Cyclohexane (analytically pure, Beijing Fine Chemicals Co., Ltd., Beijing, China) and CS_2 (analytical pure, Beijing Chemical Factory Products.).

3.2. Preparation of Catalysts

The catalysts were prepared according to the method of an industrial catalyst, except the type of zeolites, the composition of the support and the preparation method were consistent. The carrier was extruded in the proportion of Y zeolite (65 wt%) and alumina (35 wt%); then, it was dried at 393 k for 180 min and calcinated at 823 K for 180 min. The metal components in the catalyst were NiMo bimetals which were loaded via impregnation; then, they were dried at 393 k for 180 min and calcinated at 723 K for 120 min. The corresponding catalysts prepared using the zeolites were labeled CAT1, CAT2, CAT3, CAT4, CAT5, CAT6, CAT7, and CAT8.

3.3. Characterization

X-ray diffraction (XRD) measurements [12] were performed on a Bruker D5005 X′ Pert diffractometer equipped with Cu Kα radiation (λ = 1.5406 Å).

N_2 adsorption–desorption measurements were performed on a Micromeritics ASAP 2400 instrument [13].

The composition of zeolites was quantified using X-ray fluorescence (XRF) conducted on a PANalytical AxiosMAX analyzer.

The acidity was determined via the IR spectroscopy of adsorbed pyridine (Py-IR) by using a Nicolet Magna-IR 560 ESP spectrophotometer (USA) with a resolution of 1 cm^{-1}. Purified pyridine gas flowed through the catalyst at room temperature for 40 min. The IR spectra were recorded and degassed at the temperatures of 250 °C and 350 °C, respectively. The amount of acid was calculated by the following formula [23]:

$$\text{C (B-sites)} = 1.88 \times \text{IA(B)} \times R^2/W$$

$$\text{C (L-sites)} = 1.42 \times \text{IA(L)} \times R^2/W$$

in which C is the concentration (mmol/g catalyst); IA(B,L) is the integrated absorbance of the B or L band (cm^{-1}); R is the radius of the catalyst disk (cm); and W is the weight of disk (mg).

NH_3 -TPD analysis was conducted using a BEL-CAT instrument [14]. The morphology of the sulfide phase was characterized using a transmission electron microscope, Tecnai G^2F20S-TWIN [15].

Prior to the TEM analysis, the oxide samples were sulfided. After sulfidation, the temperature was decreased to room temperature under a N_2 atmosphere. Then, sulfide catalysts were suspended in cycloheptane and deposited on a carbon-coated copper grid. The WS_2 slab size distribution was determined by measuring about 700–800 particles through a reference. The average particle length ($\overline{L}$,nm) and stacking number ($\overline{N}$) were calculated according to the first moment of the distribution; the calculation equations are shown as follows:

$$\overline{L} = \frac{\sum_{i=1}^{n} n_i L_i}{\sum_{i=1}^{n} n_i} \quad (10)$$

$$\overline{N} = \frac{\sum_{i=1}^{n} n_i N_i}{\sum_{i=1}^{n} n_i} \quad (11)$$

where L_i represents the length of a single MoS_2 wafer, N_i represents the stacked layers of a single MoS_2 wafer, and n represents the number of MoS_2 wafers.

3.4. Hydrocracking Reaction

The tests were conducted in a continuously flowing tubular fixed-bed reactor loaded with 1.0 g of catalyst (~0.25 mm) diluted with the same quantity of quartz particles. Before the reaction, the catalyst was treated with sulfidation feedstock (5 wt% CS_2/cyclohexane solution) at 0.4 mL/min in the presence of 360 mL/min of hydrogen at 4.0 MPa of total pressure. Sulfidation was carried out at 633 K for 2 h, and then the feed was switched to tetralin. The reaction temperature varied from 603 K to 663 K, and the liquid flow rate was 0.1 mL/min. The reaction products were analyzed on an Agilent 6890 GC using a PONA column (50 m × 0.2 mm × 0.5 μm) and an FID detector.

4. Conclusions

The Si/Al ratio is the core property of zeolites, and the acid properties of the zeolites is based on this ratio. Therefore, two groups of molecular sieves were selected from multiple samples. The characterization results showed that in each group of zeolites, the Si/Al ratios were relatively similar, and the acid amounts characterized by NH_3-TPD were similar, while the distribution of different types acid sites characterized by Py-IR were different; meanwhile, their pore properties varied greatly. The sizes of the metal particles in the sulfidation catalysts changed slightly. The evaluation results from tetralin hydrocracking showed that increasing the proportion of V_{micro}/V_{meso} in zeolites was conducive for the production of BTEX. The hydrogenation-cracking reaction is controlled by aromatic saturation thermodynamics, and strong acidity is beneficial to the backward shift of equilibrium temperature.

Author Contributions: Data curation, Y.M.; Methodology, X.L. (Xiang Li); Project administration, Z.W.; Resources, X.L. (Xiangyun Long); Supervision, X.L. (Xiangyun Long); Writing—original draft, C.X.; Writing—review & editing, Z.C. All authors have read and agreed to the published version of the manuscript.

Funding: This research received no external funding.

Institutional Review Board Statement: Not applicable.

Informed Consent Statement: Not applicable.

Data Availability Statement: All data used during the study appear in this article.

Conflicts of Interest: The authors declare no conflict of interest.

References

1. Peng, C.; Zhou, Z.; Cheng, Z.; Fang, X. Upgrading of Light Cycle Oil to High-Octane Gasoline through Selective Hydrocracking over Non-Noble Metal Bifunctional Catalysts. *Energy Fuels* **2019**, *33*, 1090–1097. [CrossRef]
2. Peng, C.; Fang, X.C.; Zeng, R.H.; Guo, R.; Hao, W.Y. Commercial Analysis of Catalytic Hydroprocessing Technologies in Producing Diesel and Gasoline by Light Cycle Oil. *Catal. Today* **2016**, *276*, 11–18. [CrossRef]
3. Laredo, G.; Pérez-Romo, P.; Escobar, J.; Garcia-Gutierrez, J.L.; Vega-Merino, P.M. Light Cycle Oil Upgrading to Benzene, Toluene and Xylenes by Hydrocracking: Studies Using Model Mixtures. *Ind. Eng. Chem. Res.* **2017**, *56*, 10939–10948. [CrossRef]
4. Laredo, G.C.; Vega-Merino, P.M.; Hernández, P.S. Light Cycle Oil Upgrading to High Quality Fuels and Petrochemicals: A Review. *Ind. Eng. Chem. Res.* **2018**, *57*, 7315–7321. [CrossRef]
5. Calemma, V.; Giardino, R.; Ferrari, M. Upgrading of Lco by Partial Hydrogenation of Aromatics and Ring Opening of Naphthenes over Bi-Functional Catalysts. *Fuel Process. Technol.* **2010**, *91*, 770. [CrossRef]
6. Corma, A.; González-Alfaro, V.; Orchillés, A. Decalin and Tetralin as Probe Molecules for Cracking and Hydrotreating the Light Cycle Oil. *J. Catal.* **2001**, *200*, 34–44. [CrossRef]
7. Sato, K.; Iwata, Y.; Miki, Y.; Shimada, H. Hydrocracking of Tetralin over Niw/Usy Zeolite Catalysts: For the Improvement of Heavy-Oil Upgrading Catalysts. *J. Catal.* **1999**, *186*, 45–56. [CrossRef]
8. Upare, P.D.; Park, S.; Kim, M.S.; Kim, J.; Lee, D.; Lee, J.; Chang, H.; Choi, W.; Choi, S.; Jeon, Y.-P.; et al. Cobalt Promoted Mo/Beta Zeolite for Selective Hydrocracking of Tetralin and Pyrolysis Fuel Oil into Monocyclic Aromatic Hydrocarbons. *J. Ind. Eng. Chem.* **2016**, *35*, 99–107. [CrossRef]
9. Laredo, G.C.; Pérez-Romo, P.; Vega-Merino, P.M.; Arzate-Barbosa, E.; García-López, A.; Agueda-Rangel, R.; Martínez-Moreno, V.H. Effect of the Catalytic System and Operating Conditions on Btx Formation Using Tetralin as a Model Molecule. *Appl. Petrochem. Res.* **2019**, *9*, 185–198. [CrossRef]
10. Cao, Z.; Zhang, X.; Xu, C.; Huang, X.; Wu, Z.; Peng, C.; Duan, A. Selective Hydrocracking of Light Cycle Oil into High-Octane Gasoline over Bi-Functional Catalysts. *J. Energy Chem.* **2021**, *52*, 41–50. [CrossRef]
11. Park, J.I.; Lee, J.K.; Jin, M.; Kim, Y.K.; Yoon, S.H.; Mochida, I. Hydro-Conversion of 1-Methyl Naphthalene into (Alkyl)Benzenes over Alumina-Coated Usy Zeolite-Supported Nimos Catalysts. *Fuel* **2011**, *90*, 182–189. [CrossRef]
12. Shin, J.; Youngseok, O.; Yeseul, C.; Lee, J.; Kyoo, J. Design of Selective Hydrocracking Catalysts for Btx Production from Diesel-Boiling-Range Polycyclic Aromatic Hydrocarbons. *Appl. Catal. A* **2017**, *547*, 12–21. [CrossRef]
13. Escalona, G.; Rai, A.; Betancourt, P.; Sinha, A.K. Selective Poly-Aromatics Saturation and Ring Opening During Hydroprocessing of Light Cycle Oil over Sulfided Ni-Mo/SiO_2-Al_2O_3 Catalyst. *Fuel* **2018**, *219*, 270–278. [CrossRef]
14. Karakhanov, E.; Maximov, A.; Kardasheva, Y.; Vinnikova, M.; Kulikov, L. Hydrotreating of Light Cycle Oil over Supported on Porous Aromatic Framework Catalysts. *Catalysts* **2018**, *8*, 397. [CrossRef]
15. Singh, B.K.; Kim, Y.; Kwon, S.; Na, K. Synthesis of Mesoporous Zeolites and Their Opportunities in Heterogeneous Catalysis. *Catalysts* **2021**, *11*, 1541. [CrossRef]
16. Qiao, K.; Li, X.; Yang, Y.; Subhan, F.; Liu, X.; Yan, Z.; Xing, W.; Qin, L.; Dai, B.; Zhang, Z. Modification of Usy Zeolites with Malic-Nitric Acid for Hydrocracking. *Appl. Petrochem. Res.* **2016**, *6*, 353–359. [CrossRef]
17. Kazakov, M.O.; Nadeina, K.A.; Danilova, I.G.; Dik, P.P.; Klimov, O.V.; Pereyma, V.Y.; Paukshtis, E.A.; Golubev, I.S.; Prosvirin, I.P.; Gerasimov, E.Y.; et al. Influence of Usy Zeolite Recrystallization on Physicochemical Properties and Catalytic Performance of Nimo/Usy-Al_2O_3 Hydrocracking Catalysts. *Catal. Today* **2019**, *329*, 108–115. [CrossRef]
18. Nakajima, K.; Suganuma, S.; Tsuji, E.; Katada, N. Mechanism of Tetralin Conversion on Zeolites for the Production of Benzene Derivatives. *React. Chem. Eng.* **2020**, *5*, 1272–1280. [CrossRef]
19. Ren, S.; Meng, B.; Sui, X.; Duan, H.; Gao, X.; Zhang, H.; Zeng, P.; Guo, Q.; Shen, B. Preparation of Mesoporous Zeolite Y by Fluorine-Alkaline Treatment for Hydrocracking Reaction of Naphthalene. *Ind. Eng. Chem. Res.* **2019**, *58*, 7886–7891. [CrossRef]
20. Oh, Y.; Shin, J.; Noh, H.; Kim, C.; Kim, Y.S.; Lee, Y.K.; Lee, J.K. Selective Hydrotreating and Hydrocracking of Fcc Light Cycle Oil into High-Value Light Aromatic Hydrocarbons. *Appl. Catal. A* **2019**, *577*, 86–98. [CrossRef]
21. Jacobs, P.A.; Leuven, K.U. Acid Zeolites: An Attempt to Develop Unifying Concepts (P. H. Emmett Award Address, 1981). *Cat. Rev.—Sci. Eng.* **1982**, *24*, 415–440. [CrossRef]

22. Usman, M.; Li, D.; Razzaq, R.; Yaseen, M.; Li, C.; Zhang, S. Novel Mop/Hy Catalyst for the Selective Conversion of Naphthalene to Tetralin. *J. Ind. Eng. Chem.* **2015**, *23*, 21–26. [CrossRef]
23. Emeis, C.A. Determination of Integrated Molar Extinction Coefficients for Infrared Absorption Bands of Pyridine Adsorbed on Solid Acid Catalysts. *J. Catal.* **1993**, *141*, 347–354. [CrossRef]
24. Pires, J.; Fernandes, R.; Pinto, M.L.; Batista, M. Microporous Volumes from Nitrogen Adsorption at 77 K: When to Use a Different Standard Isotherm? *Catalysts* **2021**, *11*, 1544. [CrossRef]
25. Dik, P.P.; Danilova, I.G.; Golubev, I.S.; Kazakov, M.O.; Nadeina, K.A.; Budukva, S.V.; Pereyma, V.Y.; Klimov, O.V.; Prosvirin, I.P.; Gerasimov, E.Y. Hydrocracking of Vacuum Gas Oil over Nimo/Zeolite-Al_2O_3: Influence of Zeolite Properties. *Fuel* **2019**, *237*, 178–190. [CrossRef]
26. Ferraz, S.; Zotin, F.; Araujo, L.; Zotin, J.L. Influence of Support Acidity of Nimos Catalysts in the Activity for Hydrogenation and Hydrocracking of Tetralin. *Appl. Catal. A* **2010**, *384*, 51–57. [CrossRef]
27. Martinez, A.; Arribas, M.A.; Pergher, S.B. Bifunctional Noble Metal/Zeolite Catalysts for Upgrading Low-Quality Diesel Fractions via Selective Opening of Naphthenic Rings. *Catal. Sci. Technol.* **2016**, *6*, 2528–2542. [CrossRef]
28. Zhou, J.; Fan, W.; Wang, Y.; Xie, Z. The Essential Mass Transfer Step in Hierarchical/Nano Zeolite: Surface Diffusion. *Natl. Sci. Rev.* **2019**, *7*, 1630–1632. [CrossRef]
29. Contreras, M.S.; Bruin, T.D.; Mougin, P.; Toulhoat, H. Thermochemistry of 1-Methylnaphthalene Hydroconversion: Comparison of Group Contribution and Ab Initio Models. *Energy Fuels* **2013**, *27*, 5475–5482. [CrossRef]
30. Gutierrez, A.; Arandes, J.M.; Castano, P.; Aguayo, A.T.; Bilbao, J. Role of Acidity in the Deactivation and Steady Hydroconversion of Light Cycle Oil on Noble Metal Supported Catalysts. *Energy Fuels* **2011**, *25*, 3389–3399. [CrossRef]